JOURNAL OF GEOPHYSICAL RESEARCH, VOL. 105, NO. D7, PAGES 9349–9363, APRIL 16, 2000

Heat transport and weakening of atmospheric stability induced by mesoscale flows

G. A. Dalu

Cooperative Institute for Research in the Atmosphere, CIRA-CSU, Fort Collins, Colorado
Institute for Atmospheric Physics, IFA-CNR, Rome, Italy

R. A. Pielke Sr. and P. L. Vidale

Department of Atmospheric Science, Colorado State University, Fort Collins, Colorado

M. Baldi

Cooperative Institute for Research in the Atmosphere, CIRA-CSU, Fort Collins, Colorado
Institute for Atmospheric Physics, IFA-CNR, Rome, Italy

Abstract. We present an analytical evaluation and interpretation on how diabatic heating of the convective boundary layer (CBL) is transported upward into the midtroposphere by mesoscale flows, and how the air mixes with the environment and therefore weakens the atmospheric static stability. The thermodynamic imprint on the free atmosphere due to the irreversible processes such as mixing, dissipation, and diffusion, associated with the mesoscale flow, is more clearly shown when the forcing is periodic in time. Convective mixing in the CBL accounts for a thermodynamic perturbation of the order of a few degrees, while mixing associated with the mesoscale activity accounts for a perturbation of the order of half a degree. To isolate this last effect, we prescribe a periodic forcing with a 1 day period, so over 24 hours, the net diabatic input averages to zero, and the contribution due to the advection cancels out. In this formulation the perturbation is solely due to irreversible processes associated with the mesoscale. These perturbations are relevant, since they are smaller, but of the same order of magnitude as perturbations associated with mesoscale advection and the CBL mixing. A more complete evaluation of the relative contribution to the atmospheric perturbations due to the mesoscale activity was completed using an initial value problem approach. In this case, there is a net transport of the diabatic heat induced by the mesoscale flow. As a consequence, when the mesoscale flow persists for several days, the static stability of the atmosphere is eroded by the combined action of the diabatic heat, CBL mixing, and transport and mixing due to the mesoscale activity. In this paper we first evaluate the contribution of the irreversible processes using a periodic in time forcing. Then we examine the atmospheric impact due to a sequence of several sea breeze days, starting from rest at time zero and letting the flow evolve as an initial value problem. Results suggest that perturbations associated with mesoscale flows generated by landscape variability are of climatological importance and need to be introduced in a parametric form in coarser large-scale models, as presently is done with turbulent subgrid CBL processes.

1. Introduction

In regions characterized by land surface heterogeneity the lower boundary generates local atmospheric flows that redistribute momentum and diabatic heat within the planetary boundary layer (PBL) [*Avissar and Schmidt*, 1998; *Shen and Leclerc*, 1995; *Dalu et al*., 1996; *Emori*, 1998].

Integrated measurements performed during the Boreal Ecosystem-Atmosphere Study (BOREAS) experiment [*Sellers et al*., 1995] from different platforms, such as towers, balloons, and instrumented airplanes, have shown that persistent mesoscale flows can leave an imprint in the free atmosphere which extends up to the middle of the troposphere [*Pielke and Vidale*, 1995]. One important consequence is that air perturbed by the diabatic sensible heat, instead of being confined within the PBL, is transported upward and, as it diffuses, mixes with the air in the middle of the troposphere, weakening its static stability. As a result, a few days of persistency of the mesoscale flow can add up to a signal of climatological relevance [*Pielke and Vidale*, 1995].

Mesoscale flows are driven by the horizontal gradients of sensible heat fluxes, which are usually associated with landscape variability, such as due to the presence of large bodies of water, patches of terrain covered by a different kind of vegetation, and local orographic features. When the large-scale flows are weak, the surface-forced mesoscale flows, with its distinctive diurnal pattern, can persist for several days, or even weeks. The characteristics of the air above this region are affected and modified by these mesoscale winds, till they are eventually advected away by larger-scale strong atmospheric flows. Data collected during the BOREAS experiment show sizable and persistent mesoscale atmospheric flows induced by landscape variability [*Vidale et al*.,

Paper number 1999JD901064.
0148-0227/00/1999JD901064$09.00

1997]. These flows, studied by *Vidale et al*. [1997] using a numerical model (RAMS), influence the entire lower half of the troposphere through a redistribution of heat and momentum, when the large-scale conditions are favorable.

In this paper we provide a quantitative evaluation of the intensity of the perturbations induced by mesoscale flows, and of the space and timescales involved in these processes, using linear theory. Here we analyze some of the main features induced by persistent (a few days) mesoscale flows using linear theory. While only the linear response, of course, can be evaluated using linearized equations, such models have been shown to be effective in identifying dominant physical processes associated with sea breezes [e.g., *Rotunno*, 1983; *Dalu and Pielke*, 1989, 1993; *Dalu et al*., 1996]. This approach can also assist in the development of a parameterization of mesoscale effects generated by spatial variability of surface sensible heat and used in larger-scale models and as discussed by *Avissar and Chen* [1993], *Avissar and Schmidt* [1998], and *Wang et al*. [1998].

2. Governing Equations and Atmospheric Response

The two-dimensional and Boussinesq primitive equations in linear form are

$$\left(\frac{\partial}{\partial t}+\lambda\right)u - fv + \frac{\partial \phi}{\partial x} = K\left(\frac{\partial^2}{\partial x^2}+\frac{\partial^2}{\partial z^2}\right)u, \tag{1}$$

$$\left(\frac{\partial}{\partial t}+\lambda\right)v + fu = K\left(\frac{\partial^2}{\partial x^2}+\frac{\partial^2}{\partial z^2}\right)v, \tag{2}$$

$$\left(\frac{\partial}{\partial t}+\lambda\right)w + \frac{\partial \phi}{\partial z} - b = K\left(\frac{\partial^2}{\partial x^2}+\frac{\partial^2}{\partial z^2}\right)w, \tag{3}$$

$$\left(\frac{\partial}{\partial t}+\lambda\right)b + N_0^2 w = Q + K\left(\frac{\partial^2}{\partial x^2}+\frac{\partial^2}{\partial z^2}\right)b, \tag{4}$$

$$\frac{\partial u}{\partial x}+\frac{\partial w}{\partial z}=0. \tag{5}$$

As a lower boundary condition, we assume that the vertical momentum component vanishes at the ground, $w(x, z = 0, t) = 0$. In these equations, u, v, w are the velocity components, b is the buoyancy force, Q is the diabatic buoyancy source related to the vertical divergence of the sensible heat flux in the convective boundary layer (CBL), and ϕ is the geopotential as in the work of *Rotunno* [1983]. Equation (5) is the continuity equation.

We study mesoscale flows, which are diabatically forced in the CBL, as shown, for example, by *Dalu and Pielke* [1993], and how the atmospheric stability parameters can be modified by mesoscale flows on a horizontal scale of the order of two Rossby radii. When the mesoscale flows persist one or few days in weak large-scale flow conditions, the perturbation can significantly influence the lower half of the troposphere. We use the following values for the Brunt-Väisälä frequency N_0, Coriolis parameter f, and diffusion coefficient K:

$$\Theta_z = 3[\text{K/km}] \quad b = g\frac{\theta}{\Theta}, \quad N_0 = \left(g\frac{\Theta_z}{\Theta}\right)^{1/2},$$

$$K = 10 \text{ to } 100 \text{ [m}^2\text{/s]}, \tag{6}$$

$$\omega = \frac{2\pi}{\text{day}} \quad f = 2\omega \sin(54°) \qquad \lambda = 2 \text{ to } 10 \text{ [day}^{-1}\text{]}, \tag{7}$$

where θ is the potential temperature perturbation, Θ is the environment potential temperature, and Θ_z is its vertical gradient. The parameter λ^{-1} is the lifetime of the mesoscale flow; λ is a bulk dissipation that represents frictional losses at low wavenumbers, while K is the diffusion coefficient which accounts for the losses at high wave numbers.

In the presence of periodic forcing we keep the value of the diffusion coefficient constant and equal to $K = 10$ [m^2/s] and study the mesoscale response for a Rayleigh friction coefficient, $\lambda = 2$ to 10 [day^{-1}]. We conclude, from the time lag between the diabatic forcing and the mesoscale response that a realistic value of λ is closer to the higher values of the Rayleigh friction coefficient. When $\lambda = 10$ [day^{-1}], the spin-down time mesoscale flow is 2.5 hours.

The mesoscale flow is driven by the horizontal gradient of the vertical divergence of the diabatic source Q in (4):

$$Q = Q_0 q(t) r(x, z), \tag{8}$$

where $q(t)$ is its time behavior and $r(x, z)$ its spatial distribution. The equations (1)–(5) can be reduced to an equation for the stream function ψ:

$$\left[\left(\frac{\partial}{\partial t}+\lambda-K\nabla^2\right)^2+f^2\right]\frac{\partial^2\psi}{\partial z^2} + \left[\left(\frac{\partial}{\partial t}+\lambda-K\nabla^2\right)^2+N^2\right]\frac{\partial^2\psi}{\partial x^2} = -\frac{\partial Q}{\partial x},$$

$$\nabla^2 \equiv \frac{\partial^2}{\partial x^2}+\frac{\partial^2}{\partial z^2}, \qquad \frac{\partial \psi}{\partial z} = u, \qquad \frac{\partial \psi}{\partial x} = -w. \tag{9}$$

3. Atmospheric Response to a Periodic in Time Forcing

In this section we evaluate the thermodynamic imprint due to the irreversible processes. In order to isolate this contribution we apply a periodic forcing where the air particles describe closed orbits; as a result, the net diabatic input and the advection vanish over a cycle.

3.1. Diabatic Periodic Forcing

Here we assume that the diabatic forcing Q is periodic with a pulsation ω from which it follows that in a cycle the net diabatic input averages to zero:

$$Q = Q_0 \,\text{Im}\left[\frac{\exp(j\omega t)}{j}\right]\frac{1}{2}\left[1+\tanh\left(\frac{x}{L}\right)\right]\left(\frac{h-z}{h}\right)He(h-z),$$

$$Q = Q_0 \sin(\omega t)\,\frac{1}{2}\left[1+\tanh\left(\frac{x}{L}\right)\right]\left(\frac{h-z}{h}\right)He(h-z),$$

$$Q_0 = N_0^2 h\omega, \quad h = 3 \text{ km}, \quad L = 30\text{–}100 \text{ km}, \quad \Theta_z = 3 \text{ K/km}. \tag{10}$$

$He(h - z)$ is the Heaviside step function equal to 1 when $0 < z < h$ and zero when $z > h$; h is the depth of the CBL. L, ranging from 30 to 100 km, is the horizontal extent of the influence region of the mesoscale flow, and $K = 10$ m^2/s is the diffusion coefficient, and λ ranges from 2 to 10 d^{-1}.

The Fourier transform of the streamfunction equation (equation (9)), given the periodic in time forcing (equation (10)), is

$$\{[j\omega + \lambda + K(k^2 + \mu^2)]^2 + f^2\}\mu^2\tilde{\psi} + \{[j\omega + \lambda + K(k^2 + \mu^2)]^2 + N_0^2\}k^2\tilde{\psi} = \tilde{Q},$$

$$= Q_0 \frac{\frac{\pi}{2}kL}{\sinh\left(\frac{\pi}{2}kL\right)} \frac{2}{\mu}\left[1 - \frac{\sin(\mu h)}{\mu h}\right]. \quad (11)$$

In (11), $\tilde{\psi}$ is the Fourier transformed stream function, and k and μ are the horizontal and the vertical wave numbers, respectively. Solutions to (11), including momentum components, particle displacements, and temperature perturbations are given in Appendix A1.

3.2. Mesoscale Flow Intensity and Time Lag in Its Response to Forcing

Since the model is linear, the intensity of the flow increases monotonically as the forcing increases. The in-phase component φ_1 decreases monotonically as dissipation and diffusion increase, while the out-of-phase component φ_2 initially increases as dissipation and diffusion increase, to decrease monotonically for large values of dissipation and diffusion (equations (33) and (34) of Appendix A1). The flow components φ_1 and φ_1 are

$$\tilde{\varphi}_1 \sin(\omega t) + \tilde{\varphi}_2 \cos(\omega t) = \frac{\tilde{Q}[(a^2\mu^2 + b^2k^2)\sin(\omega t) - c(k^2 + \mu^2)\cos(\omega t)]}{(a^2\mu^2 + b^2k^2)^2 + c^2(k^2 + \mu^2)^2}$$

$$\approx \{\tilde{Q}[(\lambda^2 + f^2 - \omega^2)\mu^2 + N_0^2k^2]\sin(\omega t) - 2\tilde{Q}\omega\lambda(k^2 + \mu^2)\cos(\omega t)\} \cdot \{[(\lambda^2 + f^2 - \omega^2)\mu^2 + N_0^2k^2]^2 + 4\omega^2\lambda^2(k^2 + \mu^2)^2\}^{-1} \quad (12)$$

when

$$\lambda \gg K(k^2 + \mu^2).$$

While the maximum intensity of the forcing occurs at noon (equation (10)), the maximum intensity of the mesoscale flow occurs later because of the delay induced by the dissipation. The phase lag ϑ in the response can be computed from (33) and (34) of Appendix A1. The phase lag ϑ and the time lag τ_{lag} increase as the dissipation increases, and they are small at high wave numbers and large at low wave numbers; that is, small-scale mesoscale features respond quicker to forcing:

$$\vartheta = \tan^{-1}\left[\frac{\tilde{\varphi}_1}{\tilde{\varphi}_2}\right] = \tan^{-1}\left[\frac{c(k^2 + \mu^2)}{a^2\mu^2 + b^2k^2}\right] \approx -\tan^{-1}\left[\frac{2\omega\lambda\mu^2}{(\lambda^2 + f^2 - \omega^2)\mu^2 + N_0^2k^2}\right], \quad (13)$$

$$\tau_{\text{lag}} = \vartheta/\omega.$$

The values of the coefficients a, b, and c in (12) and (13) are given in (35) of the Appendix. The last formulas in (12) and (13) hold when the diffusion is small. We recall that a fully developed sea breeze has a horizontal scale of two Rossby radius, $k \approx 1/R_0$, and a vertical scale of double the CBL depth, $\mu \approx 1/h$, in (12) and in (13) [*Dalu and Pielke*, 1993], which gives a time lag $\tau_{\text{lag}} \approx [2\lambda/(\lambda^2 + f^2 - \omega^2) + N_0^2h^2/R_0^2]$. At high latitudes, the time lag between the forcing and the flow response is of the order of the lifetime of the flow; furthermore, the time lag and the phase shift are smaller at higher wave number, increase with dissipation, and decrease with latitude, vanishing in the absence of dissipation and diffusion.

Haurwitz [1947], analyzing several sea breeze cases, has empirically determined the Rayleigh friction, as $\lambda = 10\,[\text{day}^{-1}]$, as the value which induces the observed phase lag from a pure inertial oscillation in the hodograph of the horizontal wind vector. *Wang et al*. [1996] evaluate the mesoscale lifetime as λ^{-1} from 0.25 to 0.5 day, which is considerably longer than that evaluated by Haurwitz. Recently, using physical considerations, *Grant* [1997] has given as decay time $\lambda^{-1} = (u_*/h)^{-1} \approx 0.2$ day, close to Haurwitz's value.

Simulations increasing the value of the dissipation and diffusion show that the intensity of the flow decreases as the frictional force increases, while the time lag between the forcing and the mesoscale response increases for increasing values of the dissipation λ.

From (13) and from simulations the time lag τ_{lag} is from 1 to 2.5 hours for values of λ from 2 to 10 day^{-1}. Since the observed time lag between the forcing and the sea breeze response is of the order of 2–3 hours, we believe that the correct value for λ is close to that given by *Haurwitz* [1947] and by *Grant* [1997].

3.3. Thermodynamic Imprint and Air Particle Trajectories

The periodic case is not only introductory to the more complex initial value problem, but since when the forcing is periodic, the net diabatic input averages to zero in a day (equation (46)), this makes the evaluation of the net thermodynamic imprint due to irreversible processes in the free atmosphere easier to compute and clearer to understand.

In a time cycle, each air particle describes a trajectory which is a closed elongated ellipse, (Figures 1a, 2a, and 3a). The ratio between the minor and the major axis of the ellipses increases as the dissipation increases: the major axis becomes smaller as the minor axis becomes larger. Since the trajectories are closed, the net advected heat averages to zero (equation (47)). However, as the air particles describe their elliptical trajectories, they diffuse and partially mix in the environment. Each air particle interacts with the neighboring particles. The interaction distance is $r = \sqrt{K/(\lambda^2 + \omega^2)^{1/2}}$, and the timescale is $\tau = 1/\sqrt{(\lambda^2 + \omega^2)}$; see (44). The dissipative-diffusive process leaves a thermodynamic imprint with a nonzero average, (equation (48)), as shown in Figures 1b, 2b, and 3b. This imprint is of the order of tenths of degrees and may be of climatological significance, when integrated over all the coastal regions of the Earth [*Walsh*, 1974]. From (48) and (43) the temperature perturbation averaged over a cycle is

$$\overline{\delta\theta'(x,z)} = -\frac{\Theta_z}{2}\mathcal{F}^{-1}\left\{\tilde{a}_1\left[(\tilde{w}_1 + \tilde{u}_1)\frac{\partial\tilde{\zeta}_1}{\partial x} + (\tilde{w}_2 + \tilde{u}_2)\frac{\partial\tilde{\zeta}_2}{\partial x}\right] - \tilde{a}_2\left[(\tilde{w}_2 + \tilde{u}_2)\frac{\partial\tilde{\zeta}_1}{\partial z} - (\tilde{w}_1 + \tilde{u}_1)\frac{\partial\tilde{\zeta}_2}{\partial x}\right],\right\}$$

$$\cdot\,\tilde{a}_1 + j\tilde{a}_2 = \frac{[\lambda + K(k^2 + \mu^2)] - j\omega}{[\lambda + K(k^2 + \mu^2)]^2 + \omega^2} \approx \frac{\lambda - j\omega}{\lambda^2 + \omega^2} \quad (14)$$

when

$$\lambda \gg K(k^2 + \mu^2).$$

When the dissipation and diffusion are negligible, the net thermodynamic imprint is also negligible. The imprint in-

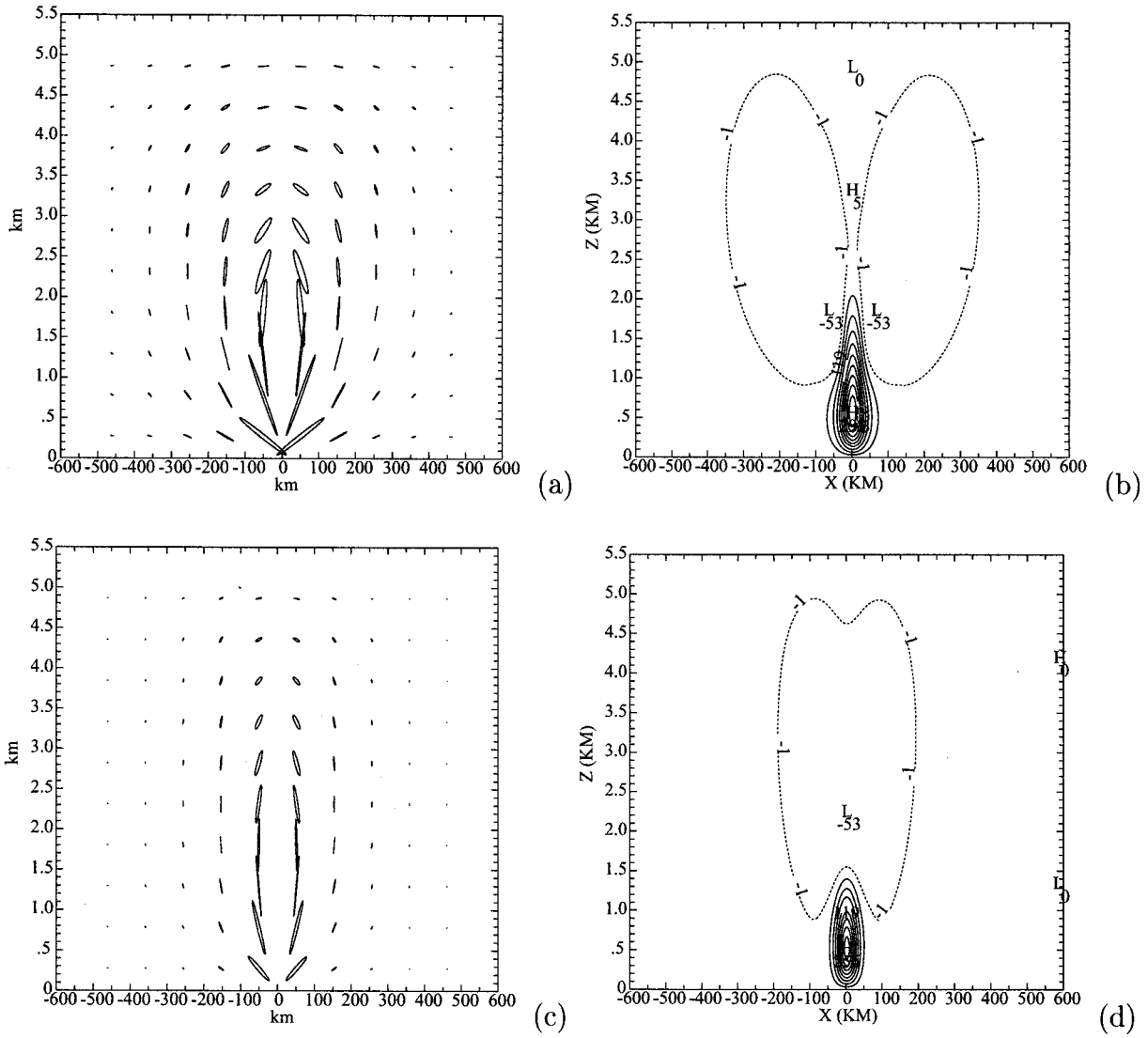

Figure 1. Air particle trajectories described for a periodic case for different values of the parameters: (a) $L_0 = 30$ km, $K = 10$ m^2/s, $\lambda = 2$ day^{-1}; and (b) averaged temperature perturbation in 1/1000 of degree. The thermodynamic imprint of the air particle trajectories is in Figure 1a. (c, d) As in Figures 1a and 1b, but $\lambda = 10$ day^{-1}.

creases with dissipation and diffusion; however, for very large values of dissipation, it decreases since the intensity of the flow decreases and the dimensions of the ellipses described by the air particles collapse. The maximum intensity of the flow and of the imprint occur when $f^2 \approx \omega^2 - [\lambda + K(k^2 + \mu^2)]^2$, which, in midlatitudes, is a value of λ close but smaller than that given by *Haurwitz* [1947] and by *Grant* [1997].

4. Diabatic Forcing in the Initial Value Problem

In this section we evaluate the thermodynamic tropospheric imprint of the mesoscale flow. We use an initial value problem approach. With a start from a rest state, we apply the diabatic forcing for four consecutive days. We evaluate the perturbations induced by the diabatic input, the advection, and the irreversible processes combined. In this section the Rayleigh friction coefficient is set to $\lambda = 5$ [day^{-1}], which corresponds to a spin-down time of the order of 5 hours in the absence of forcing. The diffusion coefficient ranges from $K = 10$ [m^2/s] to $K = 100$ [m^2/s]; larger values refer to the CBL region.

4.1. Diabatic Forcing

In the initial value problem, the atmosphere is initially unperturbed and uniformly stratified. The diabatic forcing is

$$Q(x, z, t) = Q_0 He(h - z)\,\frac{1}{2}\left[1 + \tanh\left(\frac{x}{L_0}\right)\right] \cdot [A + \sin(\omega t)], \qquad (15)$$

$$Q_0 = N_0^2 \omega h_0, \qquad L_0 = 30 \text{ km}.$$

N_0 is the Brunt-Väisälä frequency and $\omega h_0 = 2$ km/d is the growth rate of the CBL. $Q > 0$ during the daytime ($t_{\text{sunrise}} < t < t_{\text{sunset}}$), and $Q < 0$ during the night ($t_{\text{sunset}} < t < t_{\text{sunrise}}$). When $A = 0$, the duration of the day is equal to the length of the night. We chose A such as to have a daytime of 14 hours

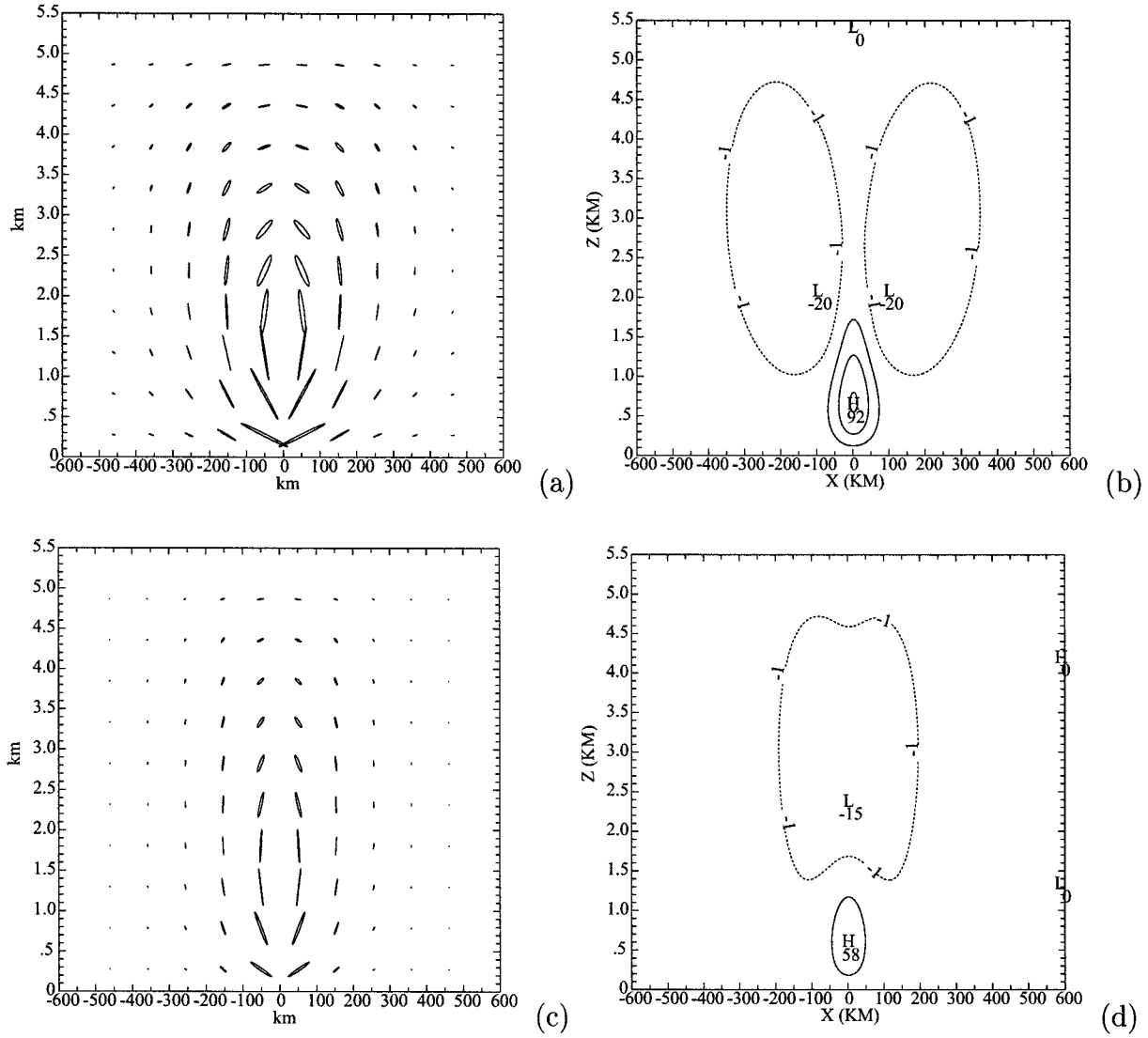

Figure 2. (a) Air particle trajectories with $L_0 = 60$ km, $K = 10$ m^2/s, $\lambda = 2$ day^{-1}; and (b) averaged temperature perturbation. The imprint of the air particle trajectories is in Figure 2a. (c, d) As in Figures 2a and 2b, but $\lambda = 10$ day^{-1}.

and a nighttime of 10 hours, as during a summer day at 54°N latitude.

During the first day ($t_{\text{sunrise}} < t < t_{\text{sunset}}$) the CBL, $h_D(x, t)$, grows monotonically from sunrise to sunset [*Green and Dalu*, 1980]:

$$h_D(x, t) = \frac{2}{N_0^2}\int_{t_{\text{sunrise}}}^{t} dt'\, Q = \frac{1}{2}\, h_{0_D}(t)\left[1 + \tanh\left(\frac{x}{L_0}\right)\right],$$
$$h_{0_D}(t) = \frac{2Q_0}{N_0^2}\left[At + \frac{1 - \cos(\omega t)}{\omega}\right]. \tag{16}$$

The diabatic heat is distributed through the CBL as

$$Q_D(x, z, t) = Q_0 He(h_{0_D}(t) - z)\,\frac{1}{2}\left[1 + \tanh\left(\frac{x}{L_0}\right)\right] \cdot [A + \sin(\omega t)]. \tag{17}$$

During the following night ($t_{\text{sunset}} < t < t_{\text{sunrise}}$) the air is cooled through a shallower layer, $h_N(x, t)$:

$$h_N(x, t) = h_{0_N}(t)\,\frac{1}{2}\left[1 + \tanh\left(\frac{x}{L_0}\right)\right], \qquad h_{0_N}(t) = 300 \text{ m}. \tag{18}$$

The diabatic cooling is distributed through the nocturnal boundary layer (NBL) as

$$Q_N(x, z, t) = Q_N He(h_{0_N}(t) - z)\,\frac{1}{2}\left[1 + \tanh\left(\frac{x}{L_0}\right)\right] \cdot [A + \sin(\omega t)]. \tag{19}$$

In the following days after the first sea breeze day, in the early hours of the morning, the convection has to work its way through the cold air of the nocturnal NBL and through the stable marine air advected inland during the night, before it can grow deeper than the CBL of the previous day. Since the depth of the density current associated with the sea breeze front is about half of the depth of the CBL of the previous day or less, this delay is $\Delta t_1 \approx 5$–6 hours, i.e., about half of the growth time of the CBL in the first day.

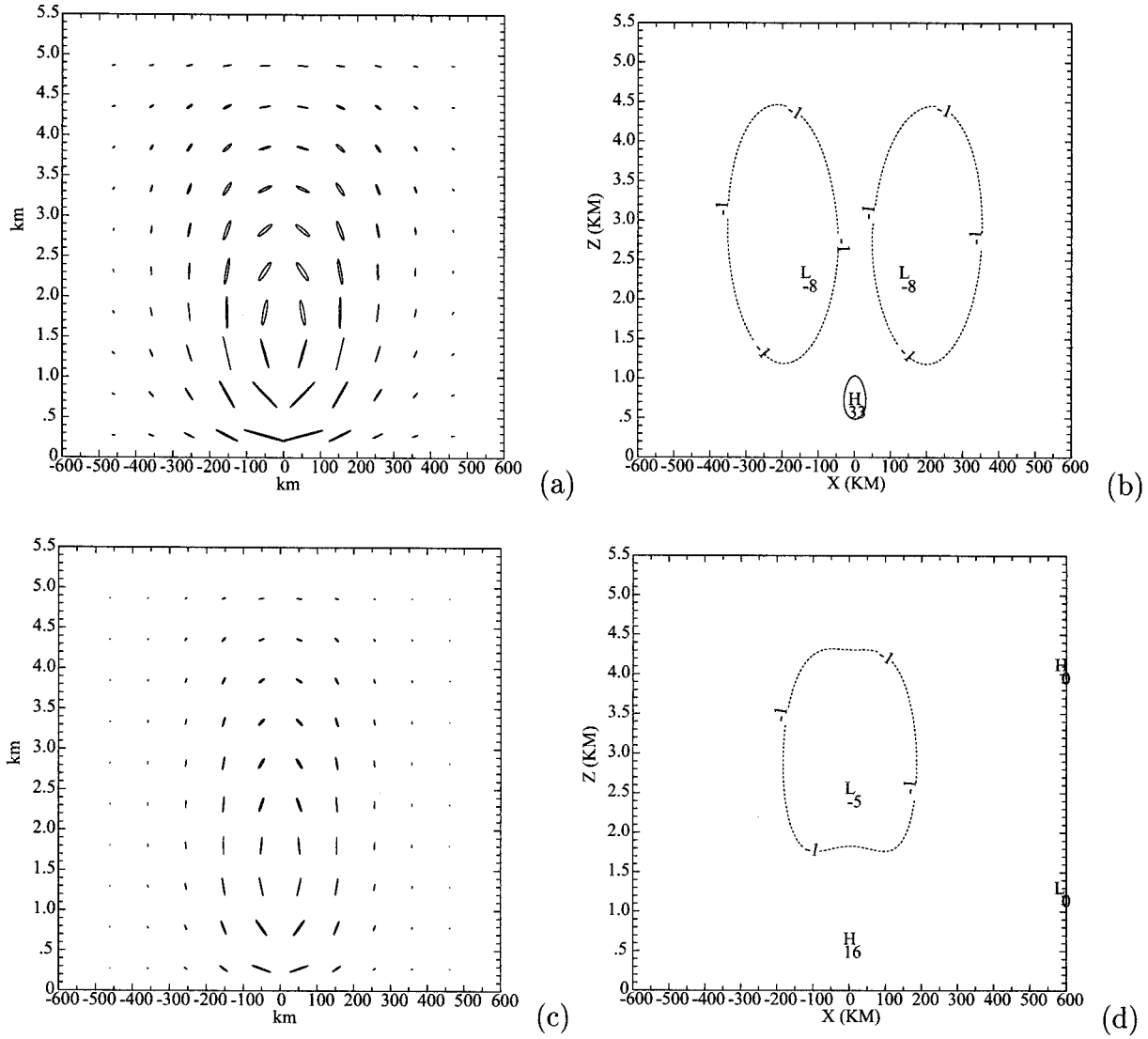

Figure 3. (a) Air particle trajectories with $L_0 = 100$ km, $K = 10$ m^2/s, $\lambda = 2$ day^{-1}, and (b) averaged temperature perturbation. The imprint of the air particle trajectories is in Figure 3a. (c, d) As in Figures 3a and 3b, but $\lambda = 10$ day^{-1}.

The behavior of the diurnal CBL, $h_{0_D}(t)$, and of the nocturnal NBL, $h_{0_N}(t)$, is shown in Figure 4, for a 4 day integration.

4.2. Stream Function and Dynamical Fields

The Fourier transform of (9), Laplace transformed in time and as forced by (15), is

$$\{[s + \lambda + K(k^2 + \mu^2)]^2 + f^2\}\mu^2\hat{\psi} + \{[s + \lambda + K(k^2 + \mu^2)]^2 + N_0^2\}k^2\hat{\psi} = Q_0 q(s) \frac{\frac{\pi}{2}kL_0}{\sinh\left(\frac{\pi}{2}kL_0\right)} \frac{2}{\mu}[1 - \cos(\mu h)], \tag{20}$$

where $\hat{\psi}$ is the stream function, and s is the Laplace transformed time t. In (20), $h = h_{0_D}(t)$ during the day, and $h = h_{0_N}(t)$ during the night. The flow driven by the diabatic input is governed by (20). The solution to the stream function equation, the momentum components, and particle displacements are given in Appendix A2.

5. Analysis of Processes in the Initial Value Problem

Taking advantage of the additivity of the solutions, because of our linear approach to the problem, here we examine the contribution of each of the physical processes in shaping the mesoscale flow.

5.1. Daytime Diabatically Driven Flow, Nighttime Diabatically Driven Flow, and Sea Breeze Fossil Flow

In daytime the flow is driven by the diabatic warming (equation (17)). The stream function and the temperature field are shown in Figure 5, at sunset of the first day (1900 LTC), which is at the end of the diurnal warming period. At this time, the sea breeze flow shows downwelling over the sea with adiabatic warming and upwelling over the land side with a lifting of the

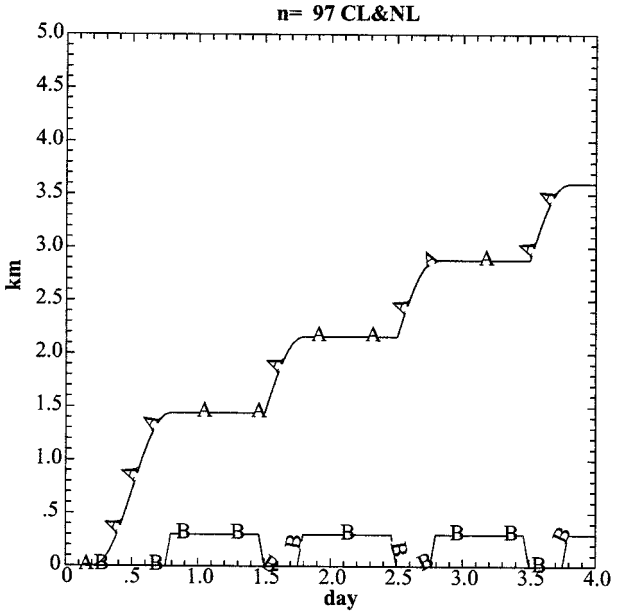

Figure 4. Initial value problem: A, depth of the convective boundary layer (CBL) depth h_{0_D}; B, depth of the nocturnal boundary layer (NBL) depth h_{0_N}.

CBL. The dynamical and thermodynamical fields are as in the work of *Dalu and Pielke* [1989].

At night the flow is driven by the diabatic cooling (equation (19)). In the early hours of the night there is strong cooling near the surface, while aloft, a fossil sea breeze flow is still active. The land breeze starts to establish itself in the lower levels, as clearly shown in Figure 6 at 2200 LTC. Across the shore the temperature horizontal gradient is negative through the depth of the nocturnal NBL, but is still positive above it, through the depth of the fossil CBL. Above the return seaward flow of the land breeze there is still the landward and the seaward flow of the fossil sea breeze. The lifetime of this fossil flow is of the order of λ^{-1}; after this period of time the sea breeze dies out, and the land breeze establishes itself in full.

5.2. Density Current and Its Energetics

As examined above, in daytime the flow is driven by the diabatic warming (Figure 5) and during the night by the diabatic cooling (Figure 6). At sunset the CBL stops growing and the diabatic diurnal warming Q_D vanishes (equations (16), (17), and Figure 4).

Here we neglect the nocturnal cooling, and we examine the adiabatic flow associated with the inland propagation of the sea breeze front [*Simpson*, 1994] and the flow associated with the diabatic warming during the following morning. The equations for the density current are given in Appendix A3 (equations (58)–(62)). The solutions are shown in (64)–(69), which are approximated in (73)–(75). The density current develops through damped inertia gravity oscillations (A3–A3), with an e-folding time $t_{\text{fold}} = \lambda^{-1}$. After the transient, $t \gg \lambda^{-1}$, i.e., when the sea breeze front is mature,

$$u_{\text{front}} \approx \overline{g'} \left[\overline{\frac{\partial h_g}{\partial x}} \right]_{x \approx L} \frac{\lambda}{\lambda^2 + f^2}, \qquad v_{\text{front}} \approx -\overline{g'} \left[\overline{\frac{\partial h_g}{\partial x}} \right]_{x \approx L} \frac{f}{\lambda^2 + f^2}, \tag{21}$$

$$L \approx L_0 + \overline{g'} \left[\overline{\frac{\partial h_g}{\partial x}} \right]_{x \approx L} \frac{\lambda(\lambda^2 + f^2)t + (f^2 - \lambda^2)}{(\lambda^2 + f^2)^2}, \tag{22}$$

where h_g is the profile of the density current (its depth), $\overline{g'}$ is the reduced gravity vertically averaged through the depth of the density current, and $[\overline{\partial h_g/\partial x}]_{x \approx L}$ is the aspect ratio of the density current near its head (Appendix A3). As quoted by *Simpson* [1994] and by *Geisler and Bretherton* [1969], u_{front} and v_{front} are of the order of 2–3 m/s. Furthermore, when the dissipation coefficient is much smaller than the inertial pulsation, $\lambda \ll f$,

$$u_{\text{front}} \approx \overline{g'} \left[\overline{\frac{\partial h_g}{\partial x}} \right]_{x \approx L} \frac{\lambda}{f^2} \approx 0, \qquad v_{\text{front}} \approx -\overline{g'} \left[\overline{\frac{\partial h_g}{\partial x}} \right]_{x \approx L} \frac{1}{f}, \tag{23}$$

$$L^2 \approx R_0^2(1 + \lambda t); \qquad \left[\overline{\frac{\partial h_g}{\partial x}} \right]_{x \approx L} \approx h_{0_D}/L. \tag{24}$$

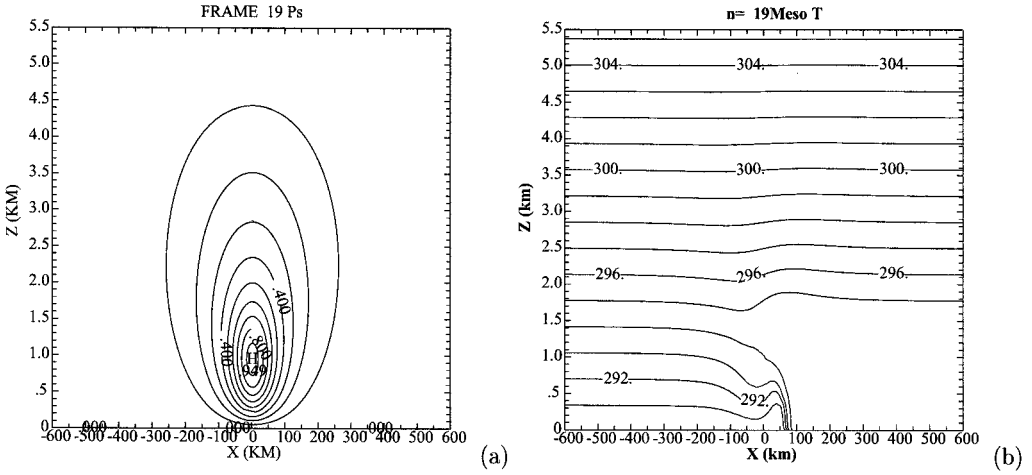

Figure 5. Initial value problem: (a) stream function, and (b) temperature field at sunset (1900 LTC) of the first day.

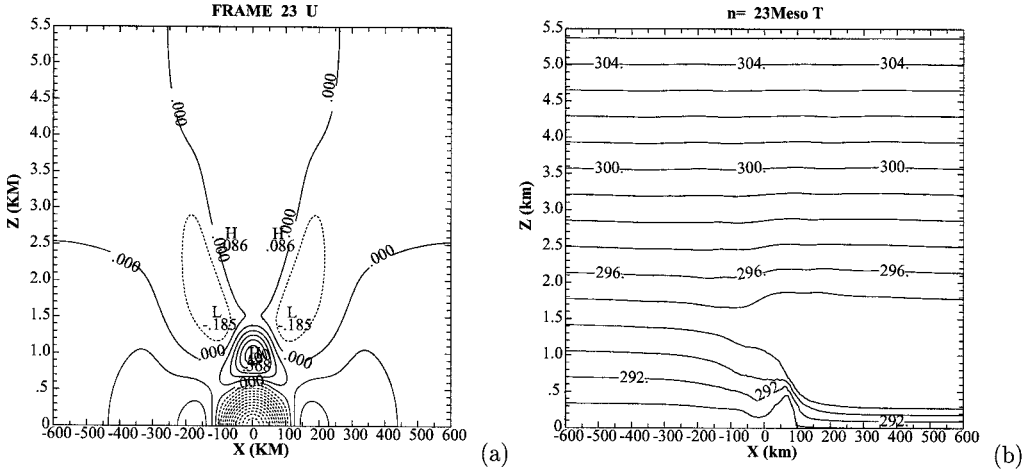

Figure 6. Initial value problem in the presence of strong nocturnal cooling: (a) stream function, and (b) temperature field at 2300 LTC of the first day.

When $\lambda \ll f$, v_{front} is in geostrophic balance, while u_{front} is almost zero, and L is of the order of the Rossby radius R_0 and still growing slowly. The flow associated with the density current is shown in Figure 7 at 1 hour after midnight.

The initial and the final mesoscale available potential energy are MAPE_i and MAPE_f, respectively, and the released energy is $\text{MAPE} = \text{MAPE}_i - \text{MAPE}_f$:

$$\text{MAPE}_i = \int_{-L_0}^{L_0} dx' \int_0^{h_g} dz'\, N_0^2(h_g - z')z' \tag{25}$$

$$= \frac{N_0^2 h_{0_D}^3}{6} \int_{-L_0}^{L_0} dx'\, h_g^3 \approx \frac{N_0^2 h_{0_D}^3}{6} \int_{-L_0}^{L_0} dx' \left(\frac{L_0 - x}{2L_0}\right)^3$$

$$= \frac{N_0^2 h_{0_D}^3}{12} L_0,$$

$$\text{MAPE}_f = \int_{-L}^{L} dx' \int_0^{h_g} dz'\, N_0^2(h_g - z')z'$$

$$\approx \frac{N_0^2 h_{0_D}^3}{6} \int_{-L'}^{L'} dx' \left(\frac{L' - x}{2L'}\right)^3 = \frac{N_0^2 h_{0_D}^3}{12} L, \tag{26}$$

$$\text{MAPE} = \text{MAPE}_i - \text{MAPE}_f = \frac{N_0^2 h_{0_D}^3}{12} [L' - L_0]$$

$$= \frac{\overline{g'} h_{0_D}^2}{12} [L - L_0], \qquad L' = \frac{L_0 + L}{2}. \tag{27}$$

The released potential energy (MAPE) linearly increases with the sea breeze penetration L. The kinetic energy released (KE) is

$$\text{KE} = \int_{-L_0}^{L} dx' \int_0^{h_D} dz'\, \frac{1}{2}[u^2 + v^2] \approx \frac{1}{2}$$

$$\cdot [u_{\text{front}}^2 + v_{\text{front}}^2] \int_{-L_0}^{L} dx' \int_0^{h_{0_D}} dz' \left[He(h_g - z)\, \frac{h_g - z}{h_g} \right.$$

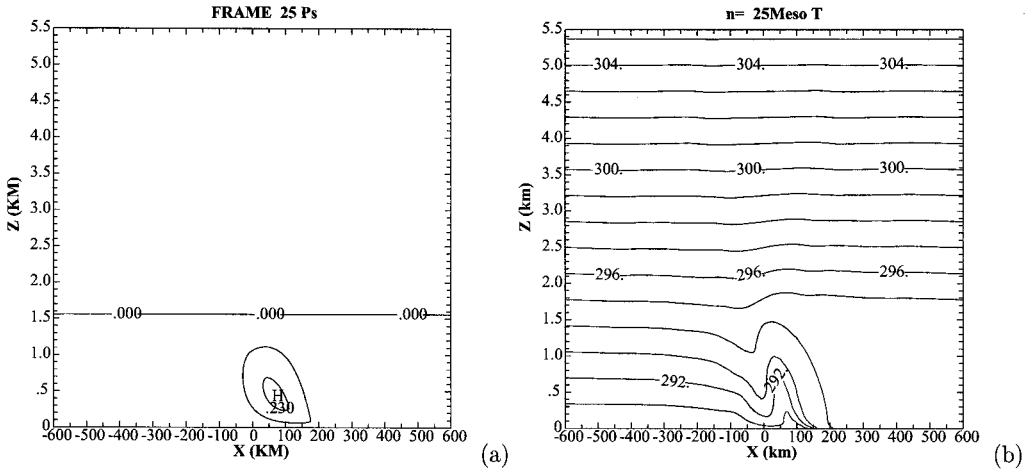

Figure 7. Initial value problem: inland penetration of the sea breeze front, negligible nocturnal cooling. (a) Stream function, (b) temperature field at 0100 LTC of the second day.

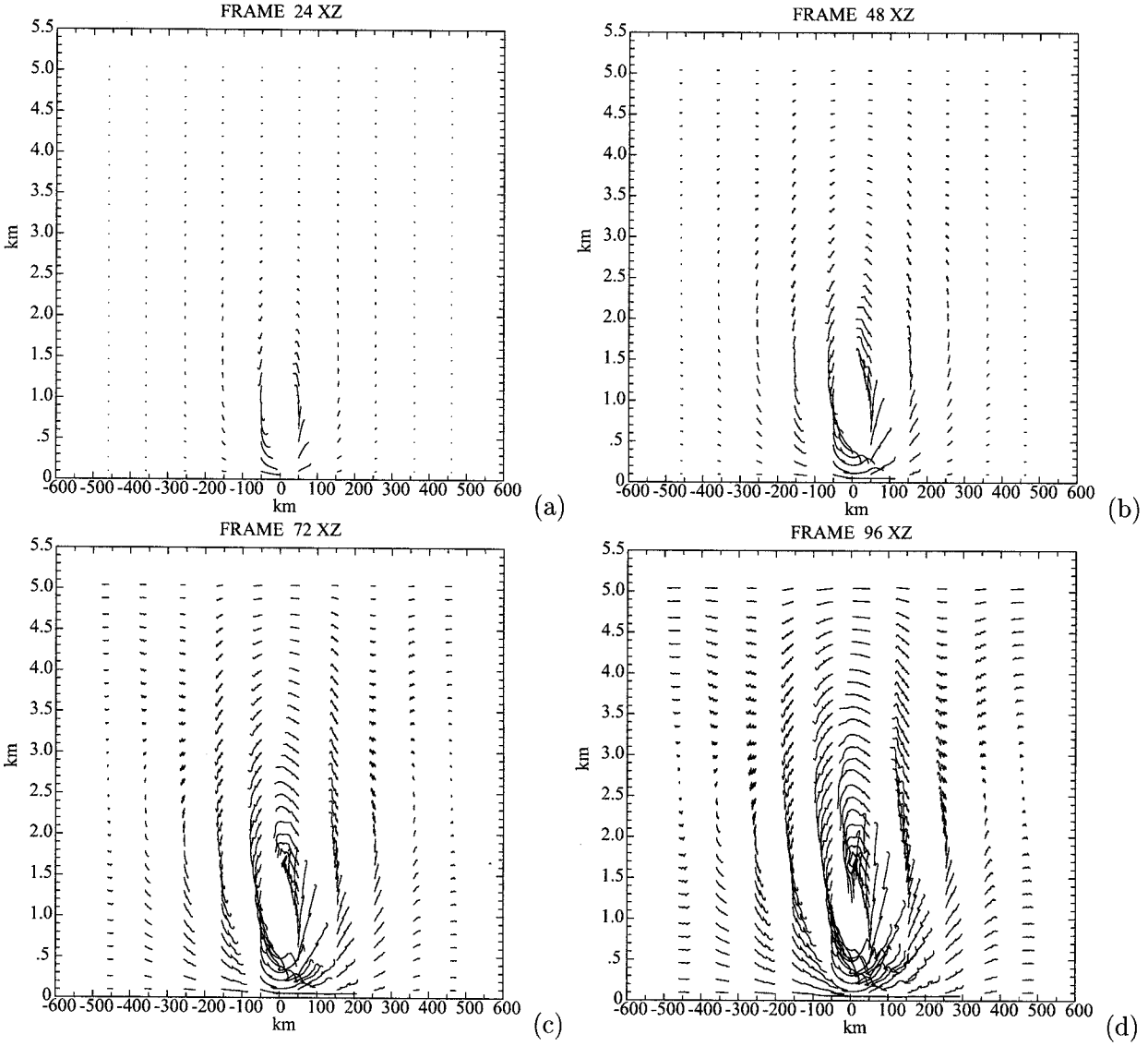

Figure 8. Initial value problem: particle trajectories at the end of each day. (a) At the end of the first day, (b) at the end of the second day, (c) at the end of the third day, and (d) at the end of the fourth day.

$$-\frac{h_g}{2h_{0_D}}\Bigg]^2\frac{1}{4}\left[1+\tanh\left(\frac{x}{L}\right)\right]^2=\frac{1}{2}\cdot[u^2_{\text{front}}+v^2_{\text{front}}]A(L,h_{0_D}). \tag{28}$$

When $t \gg \lambda^{-1}$ from Appendix A3 and (22), the kinetic energy released (KE) is

$$\text{KE}\approx\frac{\overline{g'^2}h^2_{0_D}A(L,h_{0_D})}{2L^2[\lambda^2+f^2]}. \tag{29}$$

When the dissipation is negligible, from (23), the kinetic energy (KE) released is almost twice as big, and the horizontal domain influenced is limited by the Rossby radius (maximum penetration of the front in the absence of dissipation),

$$\text{KE}\approx\frac{\overline{g'^2}h^2_{0_D}A(R_0,h_{0_D})}{2R_0^2f^2}. \tag{30}$$

The sea breeze front stops when it comes into geostrophic balance, or, in any case, at sunrise of the following day. In fact, during the early hours of the following morning, the diabatic warming (equation (17)) first erodes the stability of the inland-intruded marine air, then it further deepens the fossil CBL of the previous day (Figure 4). As the diabatic warming warms the inland-intruded marine air, the flow associated with the density current dies out, and a new diabatically driven landward flow starts to develop over the land. As the boundary layer turbulent convection becomes deeper, the temperature horizontal gradient across the shore steepens, and the flow intensifies toward the shore.

6. Heat Fluxes and Weakening of Atmospheric Stability in the Initial Value Problem

The thermal structure evolves from an initially uniformly stratified environment; Figures 9 and 10. The CBL grows dur-

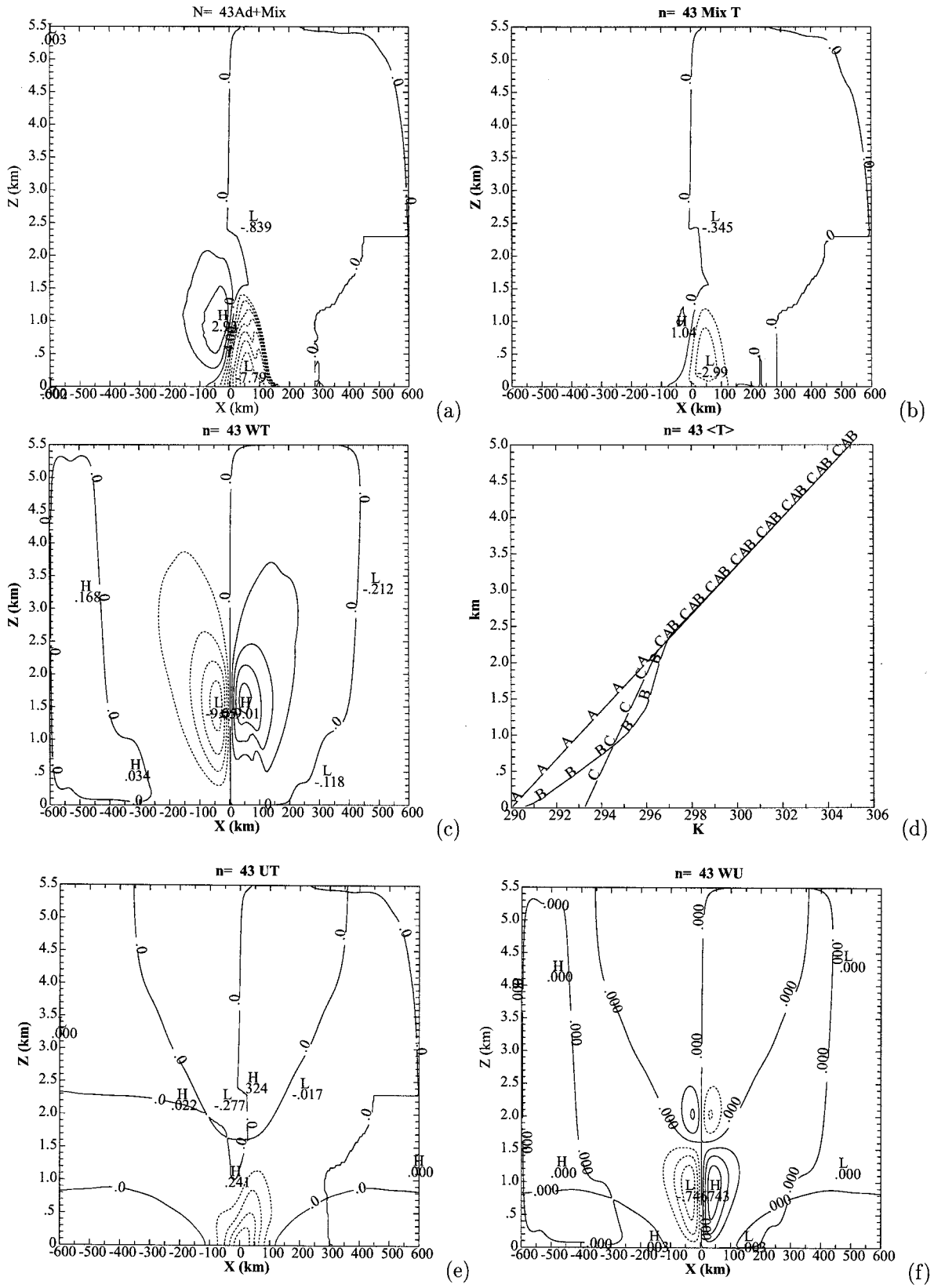

Figure 9. Initial value problem, thermodynamic features at sunset of the second day: (a) temperature perturbation due to mesoscale advection, dissipation, and diffusion; (b) temperature perturbation due only to dissipation and diffusion; (c) vertical heat flux $w\delta\theta$ (K km/d); (d) temperature vertical profiles horizontally averaged over two Rossby radii across the shore. A, initial profile; B, profile with advection and dissipation; C, profile in the absence of mesoscale flow; (e) horizontal heat flux $u\delta\theta$ (K m/s); (f) vertical flux of the horizontal momentum wu.

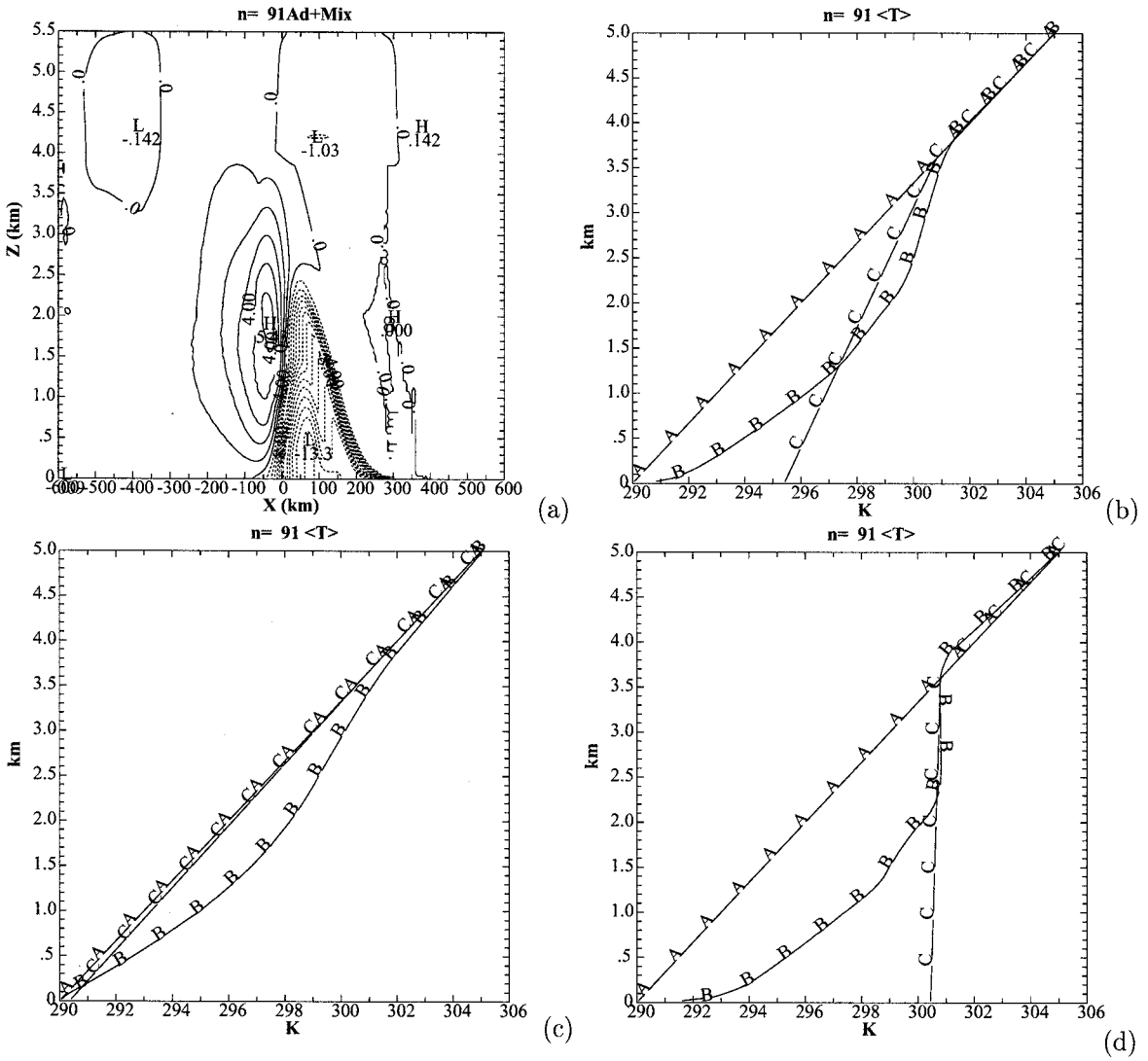

Figure 10. Initial value problem, thermodynamic features at sunset of the fourth day. (a) Temperature perturbations due to mesoscale advection, dissipation, and diffusion; (b) temperature vertical profiles horizontally averaged over two Rossby radii across the shore (A, initial profile; B, profile with advection and dissipation; C, profile in the absence of mesoscale flow); (c) temperature vertical profiles horizontally averaged over one Rossby radius over the sea (A, initial profile; B, profile with advection and dissipation; C, profile in the absence of mesoscale flow); and (d) temperature vertical profiles horizontally averaged over one Rossby radius over the land (A, initial profile; B, profile with advection and dissipation; C, profile in the absence of mesoscale flow).

ing the day (Figure 4). After sunset the CBL structure is partially eroded by the nocturnal cooling and the release of the potential energy (converted into mesoscale kinetic energy) associated with the inland penetration of the sea breeze front. During the night, through these processes the horizontal temperature gradient, built during the daylight hours, weakens, and actually can reverse below the nocturnal boundary layer because of intense nocturnal cooling. The following morning the diabatic heat warms the nocturnal boundary layer and the marine air which had penetrated inland, resetting conditions favorable to a new sea breeze event. These processes, which have been examined separately in the previous paragraph, are jointly discussed in this section.

Figure 8 shows the evolution in time of the air particle trajectories. Marine air particles move inland, cooling the air over the land side. CBL air particles are displaced upward, transporting diabatic heat and mixing in the environment. Over the sea they move downward, advecting potentially warmer air into the lower layers, and as they mix, they warm the environment; this process is adiabatic and irreversible. In the initial value problem, since the trajectories of the air particles are open, there is net transport of heat. With an idealized periodic case, the air particles describe elliptical trajectories around their equilibrium position (Figures 1a, 2a, and 3a) with zero net transport. In a daily cycle, in an initial value problem, CBL diabatic heat is transported upward, stable cool marine air moves inland in the late afternoon and during the night, where it is then diabatically heated during the daylight hours the following day. Figures 9 and 10 illustrate some of the more important thermodynamic perturbations that the mesoscale flow induces in the environment through these processes.

Figure 9 shows these features at sunset of the second day.

Figure 9a shows the temperature perturbation due to the mesoscale advection and to the mixing with about 8 K cooling over the land side and about 3 K warming over the sea side; about one third of this perturbation is due to mixing (Figure 9b). Figures 9c and 9e show the fluxes, $w\delta\theta$ and $u\delta\theta$. The vertical heat flux is negative over the sea, because potential warmer air is advected downward and is positive over the land, because diabatically warmed air is advected upward. The horizontal wind component advects marine cooler air over the land. Figure 9d shows the temperature profiles horizontally averaged over two Rossby radii centered at the shore. Over this region the static stability of the atmosphere is reinforced in the lower layer and weakened in the upper layers influenced by the mesoscale flow. Figure 9f shows that sea breezes inject horizontal momentum over land, which is removed over the sea such that they balance out.

Figure 10 shows these thermodynamics features at sunset of the fourth day. The perturbations become more and more substantial for repeated sea breeze events. Figure 10a shows a temperature perturbation, because of advection and mixing, which is about twice that of the second day. The contribution due to mixing is again about one third. Figure 10b confirms that there is strengthening of the atmospheric stability in the lower layer and weakening of stability in the upper layer over a region of two Rossby radii. Figure 10c shows the temperature profiles as averaged over the sea, and Figure 10d shows the average temperature profiles over the land. Over the sea there is substantial adiabatic warming, while over the land there is cooling in the lower layers and warming in the upper layers.

7. Conclusions

Weak large-scale ambient flows are favorable to the development of mesoscale flows driven by thermal inhomogeneities in the boundary layer. A sea-land breeze is a good example of this type of mesoscale flow. As the marine cool air moves inland, it displaces the diabatically warmed air upward. This process makes the static stability of the atmosphere stronger in the lower layers of the atmosphere and weaker in the upper layers over a region of two Rossby radii. The diabatic warming and CBL mixing is of the order of a few degrees and works toward the weakening of the stability of the lower levels of the atmosphere. The thermodynamic perturbation associated to the mesoscale advection is of the order of a few degrees, which is the order of the diabatic heating and therefore plays an important role in the redistribution of the diabatic perturbation and of momentum through the lower half of the troposphere. Diffusion and mixing associated with the mesoscale activity are important as well. These processes are adiabatic and irreversible, they leave a permanent imprint, and work toward a weakening of the average static stability of the atmosphere. The thermodynamic perturbation associated with these irreversible processes is of the order of $\frac{1}{2}$ degree. The mixing process is more intense on the land side, where it can account for as much as a third of the perturbation.

Persistent high-pressure conditions associated with weak ambient flow, such as often observed during the summer, are favorable for repeated sea-land breeze events for several days in succession. When this occurs, the perturbation due to the mesoscale flow becomes more intense as the days proceed. The affected layers become deeper, reaching the midtroposphere.

In consecutive sea breezes the sea breeze advects inland marine stable air, which is diabatically heated the following day. Each day, a volume of marine air of the order of 2 Rossby radii in the horizontal and of the order of the depth of the CBL is perturbed through this process.

The mesoscale is capable of transporting diabatic heat upward in competition with the subgrid turbulent flux. Large amounts of heat can be injected into the lower half of the troposphere through mesoscale processes, thereby changing the average large-scale characteristics of the atmosphere, such as weakening of the average static stability.

When these perturbations are not resolved explicitly, as in large-scale models, these mesoscale effects could be introduced in a parametric form using the present theory.

The simple analytical theory presented in this paper reproduces the qualitative behavior and the order of magnitude of the heat fluxes computed through a nonlinear numerical model with zero synoptic wind [*Pielke et al.*, 1991]. It also provides a framework which, when combined with the parameterization procedure introduced by *Zeng and Pielke* [1995] using a nonlinear model, can be used to develop a general procedure to parameterize mesoscale effects for use in general circulation and numerical weather prediction models.

Appendix

A1. Solutions for the Periodic Case

A1.1. Stream function. When the forcing is periodic in time (equation (10)), posing

$$\tilde{\psi}(k,\,\mu) = \tilde{\varphi}_1(k,\,\mu) + j\tilde{\varphi}_2(k,\,\mu), \tag{31}$$

the solution to the stream function (9) is given by

$$\psi(x,\,z,\,t) = \varphi_1(x,\,z)\,\sin\,(\omega t) + \varphi_2(x,\,z)\,\cos\,(\omega t), \tag{32}$$

$\varphi_1(x,\,z)$ is in phase with the forcing, as defined in (10), and $\varphi_2(x,\,z)$ is the out-of-phase component; $\varphi_1(x,\,z)$ and $\varphi_2(x,\,z)$ are the Fourier inverse transform of $\mathcal{F}^{-1}\{\tilde{\varphi}_1(k,\,\mu)\}$ and $\mathcal{F}^{-1}\{\tilde{\varphi}_2(k,\,\mu)\}$, respectively:

$$\tilde{\varphi}_1(k,\,\mu) = Q_0\,\frac{\frac{\pi}{2}\,kL}{\sinh\left(\frac{\pi}{2}\,kL\right)}\,\frac{2}{\mu}\left[1 - \frac{\sin\,(\mu h)}{\mu h}\right] \cdot \frac{a^2\mu^2 + b^2k^2}{(a^2\mu^2 + b^2k^2)^2 + c^2(k^2 + \mu^2)^2}, \tag{33}$$

$$\tilde{\varphi}_2(k,\,\mu) = -Q_0\,\frac{\frac{\pi}{2}\,kL}{\sinh\left(\frac{\pi}{2}\,kL\right)}\,\frac{2}{\mu}\left[1 - \frac{\sin\,(\mu h)}{\mu h}\right] \cdot \frac{c(k^2 + \mu^2)}{(a^2\mu^2 + b^2k^2)^2 + c^2(k^2 + \mu^2)^2}, \tag{34}$$

where

$$a^2 = [\lambda + K(k^2 + \mu^2)]^2 - \omega^2 + f^2; \qquad b^2 = [\lambda + K(k^2 + \mu^2)]^2 - \omega^2 + N_0^2; \qquad c = 2\omega[\lambda + K(k^2 + \mu^2)]. \tag{35}$$

A1.2. Momentum components and particle displacements. The horizontal and vertical momentum components are

$$u(x, z, t) = u_1(x, z) \sin(\omega t) + u_2(x, z) \cos(\omega t), \quad (36)$$

$$w(x, z, t) = w_1(x, z) \sin(\omega t) + w_2(x, z) \cos(\omega t), \quad (37)$$

where $u_1(x, z)$, $u_2(x, z)$, $w_1(x, z)$, and $w_2(x, z)$ are the Fourier inverse transform in space of $\mathcal{F}^{-1}\{\tilde{u}_1(k, \mu)\}$, $\mathcal{F}^{-1}\{\tilde{u}_2(k, \mu)\}$, $\mathcal{F}^{-1}\{\tilde{w}_1(k, \mu)\}$, and $\mathcal{F}^{-1}\{\tilde{w}_2(k, \mu)\}$, respectively:

$$\tilde{u}(k, \mu) = j\mu\tilde{\psi} = -\mu\tilde{\varphi}_2 + j\mu\tilde{\varphi}_1 = \tilde{u}_1 + j\tilde{u}_2, \quad (38)$$

$$\tilde{w}(k, \mu) = -jk\tilde{\psi} = k\tilde{\varphi}_2 - jk\tilde{\varphi}_1 = \tilde{w}_1 + j\tilde{w}_2. \quad (39)$$

The along x axis, ξ, and the along z axis, ζ, particle displacements are

$$\xi(x, z, t) = \int u(x, z, t)\, dt = \frac{1}{\omega}[u_2(x, z) \sin(\omega t) - u_1(x, z) \cos(\omega t)], \quad (40)$$

$$\zeta(x, z, t) = \int w(x, z, t)\, dt = \frac{1}{\omega}[w_2(x, z) \sin(\omega t) - w_1(x, z) \cos(\omega t)]. \quad (41)$$

The along y-axis velocity component and the along y-axis particle displacement are

$$v = -f\xi, \qquad \eta = -f \int \xi\, dt = \frac{f}{\omega^2}[u_1(x, z) \sin(\omega t) + u_2(x, z) \cos(\omega t)]. \quad (42)$$

The trajectories are ellipses, their projection into the (x, z) plane are shown in Figure 1 for different values of the dissipation, diffusion, and sea breeze front width. The air particles describe closed ellipses in a time cycle.

A1.3. Temperature perturbations. The temperature perturbation $\delta\theta(x, z, t)$ has two main contributions: the air particles are diabatically heated in the CBL and diffuse and partially merge into the environment as displaced by the mesoscale flow. The time derivative (Fourier transformed, diffusion, and dissipation included) is

$$\frac{d}{dt} \Rightarrow \mathcal{F}^{-1}\{\lambda + K(k^2 + \mu^2) + j\omega\}, \quad (43)$$

which gives

$$\left(\frac{d}{dt}\right)^{-1} \Rightarrow I(x, z) = a_1(x, z) + ja_2(x, z) \approx \frac{\pi(\lambda - j\omega)}{2\lambda K} K_0\left(\sqrt{\frac{x^2 + z^2}{r^2}}\right), \quad r^2 = \frac{2\lambda K}{\lambda^2 + \omega^2}. \quad (44)$$

The diffusion has a radius of influence equal to $r = \sqrt{2\lambda K/(\lambda^2 + \omega^2)}$, and the timescale of the diffusion is $\tau = 2\lambda/(\lambda^2 + \omega^2)$. K_0 is the zero-order K Bessel function. When the diffusion is small, the horizontal diffusion can be neglected, and

$$I(z) = a_1(z) + ja_2(z) \approx \frac{\pi r(\lambda - j\omega)}{2\lambda K} \exp\left(-\left|\frac{z}{r}\right|\right). \quad (45)$$

The approximation in (44) and (45) holds when $K(k^2 + \mu^2) < (\lambda, \omega)$, i.e., for features with wavelength larger than 1 km, which means that the approximated formula does not hold within the CBL.

Because of the diabatic forcing in the CBL (equation (10)), the temperature perturbation in the absence of mesoscale flow, $\delta\theta_D(x, z, t)$, is

$$\delta\theta_D(x, z) \sin(\omega t) = \Theta_z He(h - z)(h - z) \cdot \frac{1}{2}\left[1 + \tanh\left(\frac{x}{L}\right)\right] \sin(\omega t). \quad (46)$$

$He(h - z)$ is the Heaviside function equal to 1 when $0 < z < h$ and equal to zero when $z > 0$. L is the width of the sea breeze front.

The heated air particles, displaced by the mesoscale flow along the trajectory (ξ, ζ) (equations (40) and (41)), partially diffuse and merge into the environment, as a consequence of this Lagrangian mesoscale transport and diffusion. The diabatic perturbation $\delta\theta'_D$ becomes

$$\delta\theta'_D(x, z, t) = \int_{-\infty}^{\infty} d\xi \int_0^{\infty} d\zeta\, [a_1(x - \xi, z - \zeta) \sin(\omega t) + a_2(x - \xi, z - \zeta) \cos(\omega t)]\delta\theta_D(\xi, \zeta). \quad (47)$$

The temperature perturbation $\delta\theta'$ due to the air particles displacement through the stratified atmosphere is

$$\delta\theta'(x, z, t) = -\int \left[u \frac{\partial(\zeta\Theta_z)}{\partial x} + w \frac{\partial(\zeta\Theta_z)}{\partial z}\right] dt. \quad (48)$$

The temperature perturbation averaged over a cycle $\overline{\delta\theta'(x, z)}$ is

$$\overline{\delta\theta'(x, z)} = \frac{1}{T}\int_0^T \delta\theta'(x, z, t)\, dt, \quad (49)$$

where T is 1 day. The $\overline{\delta\theta'(x, z)}$ isolines are shown in Figure 2 for different values of the dissipation and diffusion parameters.

A2. Solutions for the Initial Value Problem

A2.1. Stream function. The solution $\hat{\psi}(k, \mu, s)$ to (20) is

$$\hat{\psi}(k, \mu, s) = Q_0 q(s) \frac{\frac{\pi}{2} kL}{\sinh\left(\frac{\pi}{2} kL\right)} \frac{2[1 - \cos(\mu h)]}{\mu} \cdot \frac{1}{\mu^2 + k^2} \frac{1}{(s + \beta)^2 + \alpha^2}. \quad (50)$$

The inverse Laplace transform of $\hat{\psi}(k, \mu, s)$ is $\tilde{\psi}(k, \mu, t)$:

$$\tilde{\psi}(k, \mu, t) = Q_0 \left\{ \frac{q(t) \frac{\pi}{2} kL}{\sinh\left(\frac{\pi}{2} kL\right)} \frac{2[1 - \cos(\mu h)]}{\mu} \cdot \frac{[\exp(-\beta t) \sin(\alpha t)]}{\alpha(\mu^2 + k^2)} \right\}, \quad (51)$$

where

$$\{f(t)\,g(t)\} = \int_0^t dt\, f(t-t')\,g(t')$$

denotes a convolution product in time.

We recall that k and μ are the horizontal and the vertical wavenumber, respectively, and s is the time Laplace transform, α is the pulsation of the wave with $[k,\ \mu]$ as horizontal and vertical wave numbers; β^{-1} is the lifetime:

$$p = s + \lambda + K(k^2+\mu^2) = s + \beta, \qquad \beta = \lambda + K(k^2+\mu^2),$$
$$\alpha = \frac{f^2\mu^2 + N_0^2k^2}{\mu^2+k^2}, \quad a^2 = p^2 + f^2; \quad b^2 = p^2 + N_0^2. \tag{52}$$

A2.2. Momentum components and particle displacement. The momentum components are

$$\tilde{u}(k,\ \mu,\ t) = j\mu\tilde{\psi}(k,\ \mu,\ t), \qquad \tilde{w}(k,\ \mu,\ t) = -jk\tilde{\psi}(k,\ \mu,\ t), \tag{53}$$

and the particle displacements are

$$\tilde{\xi}(k,\ \mu,\ t) = \int_0^t dt'\ \tilde{u}(k,\ \mu,\ t')$$
$$\tilde{\zeta}(k,\ \mu,\ t) = \int_0^t dt'\ \tilde{w}(k,\ \mu,\ t'). \tag{54}$$

The along y axis velocity component and particle displacement are:

$$\tilde{v}(k,\ \mu,\ t) = -f\tilde{\xi}(k,\ \mu,\ t)$$
$$\tilde{\zeta}(k,\ \mu,\ t) = \int_0^t dt'\ \tilde{v}(k,\ \mu,\ t'). \tag{55}$$

A2.3. Temperature perturbations. The temperature perturbation $\delta\theta(x,\ z,\ t)$ has several contributions since the air particles are diabatically heated (cooled during the night) in the PBL, and partially merge into the environment as displaced by the mesoscale flow. In our initial value formulation the time derivative, with diffusion and dissipation included, is

$$\frac{d}{dt} \Rightarrow p = s + \lambda + K(k^2+\mu^2),$$

while its inverse, Laplace and Fourier inverted, gives the Gaussian diffusion:

$$I(x,\ z,\ t) = \mathcal{L}^{-1}\mathcal{F}^{-1}\left\{\frac{1}{s+\lambda+K(k^2+\mu^2)}\right\}$$
$$= \frac{\pi}{Kt}\exp\left[-(\lambda t)\right]\exp\left[-\left(\frac{x^2+z^2}{4r^2}\right)\right]$$
$$\approx \sqrt{\frac{\pi}{Kt}}\exp\left[-(\lambda t)\right]\exp\left[-\left(\frac{z^2}{4r^2}\right)\right]; \quad r^2 = Kt. \tag{56}$$

During the diurnal hours the depth of the CBL grows, and the particles are heated as they are displaced and diffused through the environment. Just before sunset the CBL stops growing, while the front continues to expand at the rate of about a Rossby radius per day and, furthermore, during the night the particles are diabatically cooled. The resulting temperature perturbation, $\delta\theta(x,\ z,\ t)$, is

$$\delta\theta = \omega h_0\Theta_z \int_0^t dt' \int_{-\infty}^{\infty} d\xi \int_0^{h(t')} d\zeta\, \frac{1}{2}\left[1+\tanh\left(\frac{\xi}{L}\right)\right]$$
$$\cdot\,[A+\sin(\omega t')]I(x-\xi,\ z-\zeta,\ t-t'), \tag{57}$$

where $h(t)$ is the depth of the CBL during the day and the depth of the cold surface layer at night.

A3. Density Current

The density current behavior is governed by the following set of equations:

$$h_g(x,\ t) = \frac{1}{2}\left[1-\tanh\left(\frac{x}{L}\right)\right]h_{0_D}(t = t_{\text{sunset}}) \tag{58}$$

where

$$L = L_0 + \int u_{\text{front}}\, dt,$$

$$\left(\frac{\partial}{\partial t}+\lambda\right)u - fv = g'\frac{\partial h_g}{\partial x} \Rightarrow (s+\lambda)u - fv = g'\frac{\partial h_g}{\partial x}, \tag{59}$$

$$\left(\frac{\partial}{\partial t}+\lambda\right)v + fu = 0 \Rightarrow (s+\lambda)v + fu = 0, \tag{60}$$

$$\frac{\partial u}{\partial x} + \frac{\partial w}{\partial z} = 0, \tag{61}$$

$$\text{B.C.s} \Rightarrow w(x,\ z,\ t)\big|_{z=0} = 0, \qquad w(x,\ z,\ t)\big|_{z=h_{0_D}} = 0. \tag{62}$$

As boundary conditions, we assume that the vertical velocity component vanishes at the ground and at the top of the CBL. The reduced gravity g' and the vertically averaged reduced gravity $\overline{g'}$ are

$$g' = N_0^2 He(h_g - z)(h_g - z), \qquad \overline{g'} = \frac{1}{2}N_0^2 h_{0_D}, \tag{63}$$

where h_g is the depth of the density current. Equations (58)–(62) are solved using the Laplace transform theory.

From (59) to (61) the velocity components $(u_g,\ v_g,\ w_g)$ within the gravity current, $z < h_g$, are

$$u_g = N_0^2 h_{0_D} He(h_g - z)\,\frac{h_g - z}{h_g}\left\{\frac{\partial h_g}{\partial x}\exp(-\lambda t)\cos(ft)\right\}, \tag{64}$$

$$v_g = -N_0^2 h_{0_D} He(h_g - z)\,\frac{h_g - z}{h_g}\left\{\frac{\partial h_g}{\partial x}\exp(-\lambda t)\sin(ft)\right\}, \tag{65}$$

$$w_g = -\int_0^z dz\,\frac{\partial u_g}{\partial x} = -N_0^2 h_{0_D} He(h_g - z)$$
$$\cdot\,\frac{h_g z - 0.5z^2}{h_g}\left\{\frac{\partial^2 h_g}{\partial x^2}\exp(-\lambda t)\cos(ft)\right\}. \tag{66}$$

Given the B.C.s, (62), the return flow, $z < h_{0_D}$, is

$$u_r = -\frac{1}{h_{0_D}}\int_0^{h_g} dz\, u_g, \quad v_r = -\frac{1}{h_{0_D}}\int_0^{h_g} dz\, v_g, \quad w_r = -\int_0^{h_g} dz\, \frac{\partial u_r}{\partial x}. \tag{67}$$

Finally, the velocity components are

$$u(x,z,t) = u_g + u_r, \quad v(x,z,t) = v_g + v_r, \quad w(x,z,t) = w_g + w_r, \tag{68}$$

while the front velocity u_{front} and the across front velocity v_{front} are,

$$u_{\text{front}} = \frac{1}{L}\int_{-\infty}^{L} dx\, \frac{1}{h_g}\left[\int_0^{h_g} dz\, u\right], \qquad v_{\text{front}} = \frac{1}{L}\int_{-\infty}^{L} dx\, \left[\frac{1}{h_g}\int_0^{h_g} dz\, v\right]. \tag{69}$$

Considering that the aspect ratio of the frontal region of the see breeze is almost conserved and is of the order of 0.5 [*Simpson*, 1994], $[\overline{\partial h_g/\partial x}]_{x\approx L} = \mathrm{O}(0.5)$, the above equations can be approximated as

$$u_{\text{front}}(t) \approx \overline{g'}\left[\frac{\overline{\partial h_g}}{\partial x}\right]_{x\approx L} \frac{\lambda + \exp(-\lambda t)[f\sin(ft) - \lambda\cos(ft)]}{\lambda^2 + f^2}, \tag{70}$$

$$v_{\text{front}}(t) \approx -\overline{g'}\left[\frac{\overline{\partial h_g}}{\partial x}\right]_{x\approx L} \frac{f - \exp(-\lambda t)[\lambda\sin(ft) + f\cos(ft)]}{\lambda^2 + f^2}, \tag{71}$$

$$L(t) \approx L_0 + \overline{g'}\left[\frac{\overline{\partial h_g}}{\partial x}\right]_{x\approx L} \cdot\{\lambda t(\lambda^2 + f^2) + (f^2 - \lambda^2) - \exp(-\lambda t) \cdot[2f\lambda\sin(ft) + (f^2 - \lambda^2)\cos(ft)]\} \cdot[(\lambda^2 + f^2)^2]^{-1}. \tag{72}$$

The density current penetrates inland through inertial damped oscillations, with a pulsation equal to f. In the presence of dissipation the inertia gravity oscillations have an e-folding time $t_{\text{fold}} = \lambda^{-1}$. The velocity components are

$$u(x,z,t) \approx v_{\text{front}}(t)\, He(h_{0_D} - z) \cdot\left[He(h_g - z)\,\frac{h_g - z}{h_g} - \frac{h_g}{2h_{0_D}}\right]\frac{1}{2}\left[1 + \tanh\left(\frac{x}{L}\right)\right], \tag{73}$$

$$v(x,z,t) \approx v_{\text{front}}(t)\, He(h_{0_D} - z) \cdot\left[He(h_g - z)\,\frac{h_g - z}{h_g} - \frac{h_g}{2h_{0_D}}\right]\frac{1}{2}\left[1 + \tanh\left(\frac{x}{L}\right)\right], \tag{74}$$

$$w(x,z,t) = -\int_0^z \frac{\partial u(x,z,t)}{\partial x}\, dz. \tag{75}$$

Acknowledgments. G. A. Dalu and M. Baldi acknowledge the support of the Italian ASI Project and the Cooperative Institute for Research in the Atmosphere (CIRA). Support was also provided by the NSF under ATM-9306754 and ARO grant DAAL01-98-2-0078. This work was completed during visits of G. A. Dalu and M. Baldi to Colorado State University. Dallas McDonald very capably handled the final preparation of the paper.

References

Avissar, R., and F. Chen, Development and analysis of prognostic equations for mesoscale kinetic energy and mesoscale (subgrid-scale) fluxes for large-scale atmospheric models, *J. Atmos. Sci.*, *50*, 3751–3774, 1993.

Avissar, R., and T. Schmidt, An evaluation of the scale at which ground-surface heat flux patchiness affects the convective boundary layer using large eddies simulations, *J. Atmos. Sci.*, *55*, 2666–2689, 1998.

Dalu, G. A., and R. A. Pielke, An analytic study of the sea breeze, *J. Atmos. Sci.*, *46*, 1815–1825, 1989.

Dalu, G. A., and R. A. Pielke, Vertical heat fluxes generated by mesoscale atmospheric flow induced by thermal inhomogeneities in the PBL, *J. Atmos. Sci.*, *50*, 919–926, 1993.

Dalu, G. A., R. A. Pielke, M. Baldi, and X. Zeng, Heat and momentum fluxes induced by thermal inhomogeneities, *J. Atmos. Sci.*, *53*, 3286–3302, 1996.

Emori, S., The interaction of cumulus convection with soil moisture distribution: An idealized simulation, *J. Geophys. Res.*, *103*, 8873–8884, 1998.

Geisler, J., and F. P. Bretherton, The sea breeze front runner, *J. Atmos. Sci.*, *26*, 82–95, 1969.

Grant, A. L. M., An observational study of the evening transition boundary-layer, *Q. J. R. Meteorol. Soc.*, *123*, 657–677, 1997.

Green, J. A. S., and G. A. Dalu, Mesoscale energy generated in the boundary layer, *Q. J. R. Meteorol. Soc.*, *106*, 721–726, 1980.

Haurwitz, B., Comments on the sea-breeze circulation, *J. Meteorol.*, *4*, 1–8, 1947.

Pielke, R. A., and P. L. Vidale, The boreal forest and the polar front, *J. Geophys. Res.*, *100*, 25,755–25,758, 1995.

Pielke, R. A., G. A. Dalu, J. S. Snook, T. J. Lee, and T. G. F. Kittel, Nonlinear influence of mesoscale land-use on weather and climate, *J. Clim.*, *4*, 1053–1069, 1991.

Rotunno, R., On the linear theory of land and sea breeze, *J. Atmos. Sci.*, *40*, 1999–2009, 1983.

Sellers, P. J., et al., The Boreal Ecosystem-Atmosphere Study (BOREAS): An overview and early results from the 1994 field year, *Bull. Am. Meteorol. Soc.*, *76*, 1549–1577, 1995.

Shen, S., and M. Y. Leclerc, How large must surface inhomogeneities be before they influence the convective boundary layer structure, A case study, *Q. J. R. Meteorol. Soc.*, *121*, 1209–1228, 1995.

Simpson, J. E., *Sea Breeze and Local Wind*, 234 pp., Cambridge Univ. Press, New York, 1994.

Vidale, P. L., R. A. Pielke, A. Barr, and L. T. Steyaert, Case study modeling of turbulent and mesoscale fluxes over the BOREAS region, *J. Geophys. Res.*, *102*, 29,167–29,188, 1997.

Walsh, J., Sea breeze theory and applications, *J. Atmos. Sci.*, *31*, 2012–2026, 1974.

Wang, J., R. L. Bras, and E. A. B. Eltahir, A stochastic linear theory of mesoscale circulation induced by the thermal heterogeneity of the land surface, *J. Atmos. Sci.*, *53*, 3349–3366, 1996.

Wang, J., E. A. B. Eltahir, and R. L. Bras, Numerical simulation of nonlinear mesoscale circulations induced by the thermal heterogeneities of land surface, *J. Atmos. Sci.*, *55*, 447–464, 1998.

Zeng, X., and R. A. Pielke, Further study on the predictability of landscape-induced atmospheric flow, *J. Atmos. Sci.*, *52*, 1680–1698, 1995.

M. Baldi, Cooperative Institute for Research in the Atmosphere, CIRA-CSU, Fort Collins, CO 80523.

G. A. Dalu, Institute for Atmospheric Physics, IFA-CNR, I-00133 Tor Vergata Rome, Italy.

R. A. Pielke Sr. and P. L. Vidale, Department of Atmospheric Science, CSU, Foothill Campus, Fort Collins, CO 80523. (dallas@cobra.atmos.colostate.edu)

(Received January 22, 1999; revised September 10, 1999; accepted September 28, 1999.)